Available online at www.sciencedirect.com
SCIENCE DIRECT
International Journal of Heat and Mass Transfer 49 (2006) 2173–2179
International Journal of HEAT and MASS TRANSFER
www.elsevier.com/locate/ijhmt

Large eddy simulation (LES) for synthetic jet thermal management

Yong Wang [a], Guang Yuan [b], Yong-Kyu Yoon [b], Mark G. Allen [b], Sue Ann Bidstrup [a,*]

[a] School of Chemical and Biomolecular Engineering, Georgia Institute of Technology, Atlanta, GA 30332-0100, United States
[b] School of Electrical and Computer Engineering, Georgia Institute of Technology, Atlanta, GA 30332-0250, United States

Received 1 June 2005; received in revised form 23 November 2005
Available online 9 March 2006

Abstract

An active cooling substrate (ACS) is a microelectro mechanical system (MEMS) device which implements the synthetic jet concept into printed wiring board (PWB) to enhance thermal management. This paper presents a numerical approach to solve the synthetic jet fluid mechanics and heat transfer problem. Fluent, a computational fluid dynamics (CFD) package, is utilized to perform the three-dimensional (3-D), unsteady, and double precision simulations. The large eddy simulation (LES) is selected as the turbulence model. The simulation results are consistent with the experimental data. A numerical predictive model is developed for future designs of synthetic jet based active cooling substrates.

Keywords: Synthetic jet; Active cooling substrate; Large eddy simulation

1. Introduction

A synthetic jet is formed from a train of vortex rings or pairs, created in the external fluid, without net mass addition [1]. The device which produces this jet consists of a cavity with rigid side walls, an oscillating diaphragm and a rigid cap with an orifice. Fig. 1 shows the basic synthetic jet concept. When the diaphragm is vibrated rapidly, air is repeatedly drawn into the cavity through the orifice and then ejected out of the cavity through the same orifice. As the outgoing flow passes the sharp edges of the orifice, the flow separates, forming a vortex ring which propagates normally away from the orifice plate. One vibration cycle can be divided into an impingement stroke and an intake stroke. On the impingement stroke, the diaphragm deflects upward to compress the fluid in the cavity. The increase in pressure drives the fluid out through the orifice. On the intake stroke, the diaphragm deflects in the opposite direction, and the cavity acts as a sink to entrain the fluid back into it from all the directions.

Synthetic jets have seen widespread laboratory use in flow control [2,3]. Utility of synthetic jets in microsystem packaging to enhance thermal management is a newly emerging application. A synthetic jet can be used in a microelectronic thermal packaging because of its two unique natures: vortex structures and zero-net-mass-flux. The train of the vortex rings has the ability to entrain surrounding low momentum fluid into the jet core. An increase in the jet flow can carry away more heat. In addition, vortex rings induce disturbances into the jet flow which facilitates the breakup of the boundary layer. Laminar flow exists in the boundary layer, and heat conduction is the dominant heat transfer mode. With a thinner boundary layer, heat convection is enhanced with respect to heat conduction. Zero-net-mass-flux jets require no mass addition to the system and thus provide means of efficiently directing airflow across a heated surface. Because these jets are zero net mass flux in nature and are comprised entirely of the ambient fluid, they can be conveniently integrated with the surfaces that require cooling without the need for complex plumbing. This simple structure eases the integration of synthetic jet with current packaging components. Fig. 2 shows an example of the implementation of

* Corresponding author. Tel.: +1 404 894 5053; fax: +1 404 894 2866.
E-mail address: sue.allen@carnegie.gatech.edu (S.A. Bidstrup).

0017-9310/$ - see front matter © 2006 Elsevier Ltd. All rights reserved.
doi:10.1016/j.ijheatmasstransfer.2005.11.024

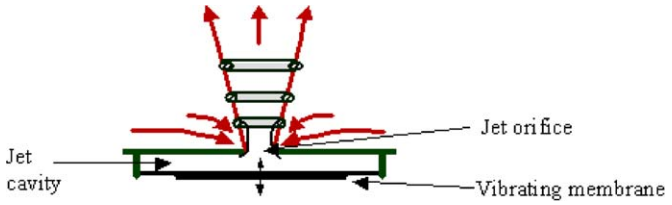

Fig. 1. Schematic of a synthetic jet.

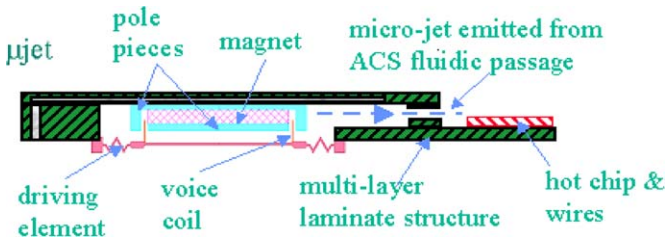

Fig. 2. Schematic of an active cooling substrate in printed wiring board.

the synthetic jet technology. A synthetic jet unit is embedded in the printed wiring board substrate. Microfluidic channels are fabricated in the substrate to vector the jet to the on-demand cooling locations. A polymeric corrugated diaphragm is laminated on the substrate. The vibration of the diaphragm is excited by an electromagnetic driver which consists of a permanent magnet glued at the center of the cavity and a self-supporting coil attached at the rigid center of the polymeric diaphragm. This membrane actuator synthetic jet can offer pin-point cooling to eliminate hot spots on the integrated circuit chip and enhance cooling functionality of the conventional printed wiring board. This device is referred to as active cooling substrate (ACS) [4–6].

Computational fluid mechanics can be used to provide a better understanding of the complex fluid physics and to provide predictive models for engineering analysis. The modeling can reduce the cost and time needed to develop a prototype. Numerical simulation studies on the synthetic jet fluid mechanics behavior have been performed by [7–9]. In synthetic jets, fluid ejected by the pulsing jets rolls upward into vortices that propagate due to their mutually induced velocity and the initial momentum given by the pulse. To capture the unique flow features of the synthetic jets, the pulsating boundary condition must be set.

The flexible diaphragm is a pulsating boundary. Rizzetta et al. [7] simulated the membrane motion by varying the position of appropriate boundary points. Lee and Goldstein [8] used a virtual surface to define the moving wall. This approach imposes a localized body force along desired points in the computational mesh to bring the fluid there to a specified velocity so that the force has the same effect as a solid boundary. The desired velocity is incorporated in an iterative feedback loop to determine the appropriate force. This technique allows for fairly complex geometries and/or moving boundaries to be incorporated in a regular domain without the usual complexities of mapping. Another simplified alternative is to apply an analytical velocity profile on the boundary region. Kral et al. [9] directly applied a suction/blowing type velocity boundary on the region corresponding to the jet orifice. The perturbation on the flow field is introduced through the wall normal component of velocity as shown in Eq. (1):

$$\overline{u_n}(\xi = 0, \eta, t) = U_0 f(\eta) \sin(\omega t) \tag{1}$$

where U_0 is the magnitude of the velocity, ξ denotes the streamwise direction, η denotes the cross-stream direction, and $\overline{u_n}$ is the streamwise component of velocity. $f(\eta)$ represents different spatial variations over the orifice. The validity of this approach has been confirmed by the moving wall technique. Therefore, this simplified boundary condition can dramatically reduce the computational time compared to the conventional boundary condition of a solid moving surface.

The second challenge of the synthetic jet simulations is to combine fluid mechanics with heat transfer. In this research, synthetic jets are employed in thermal management. Thus, it is necessary to ascertain the impact of fluid physics on heat transfer. Chiriac et al. [10] simulated the heat removal of the unsteady impinging jets. A uniform heat flux boundary is added to the simulation model. Compared to the steady impinging jets, the unsteady jet becomes distorted and buckles beyond a critical Reynolds number of 600, which leads to a sweeping motion of its tip. As a result of the combined buckling/sweeping jet motion, the cooled area is significantly enhanced.

In this study, due to the microsystem packaging application, a low profile design is required. Therefore, the ACS device is embedded in the thickness of the substrate and generates a tangential jet to remove the heat. The simulation problem of synthetic jet fluid mechanics combined with heat transfer is explored by using a commercial CFD software package, Fluent. This is the first comprehensive CFD study comprising the jet formation, development and the interaction of its flow pattern and heat transfer phenomena. In the following sections, the simulation approach and results are discussed.

2. Simulation approach

There are two basic steps involved in a CFD simulation: (1) drawing and gridding the physical model; (2) applying boundary conditions and solving the problem. Fluent Inc. offers another software package, GAMBIT, to accomplish the model drawing and meshing. Fig. 3 shows the symmetric cross-section view of the 3-D meshed model for the ACS device with a rectangular fluidic channel exit of 5.08 mm × 1.00 mm. The model dimensions are exactly the same as the actual ACS device. There is a quarter of a sphere attached at the jet outlet to explore the jet development at the downstream. This dome does not exist in a real case; however, it is defined in the simulation to investigate the flow field at the downstream of the jet outlet. The flow field developed inside the dome, especially the ACS

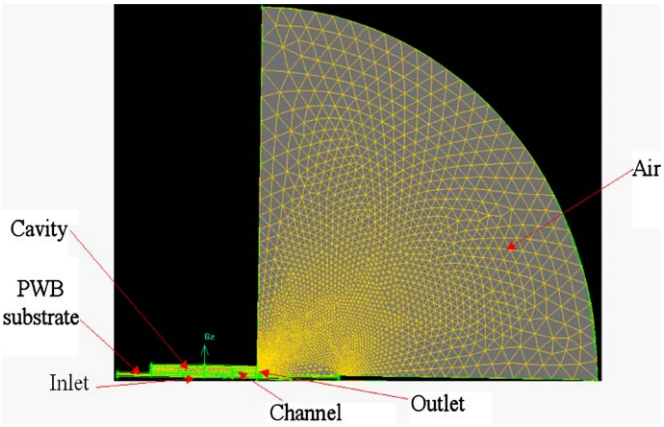

Fig. 3. CFD model for fluid mechanics and heat transfer simulation.

channel exit proximity region, is the focus of the CFD simulations. In order to eliminate the edge effect of the dome on the jet behavior, the dome radius is selected as 20 times larger than the width of the jet exit. To account for heat conduction, the physical model should include the printed wiring board substrate. Therefore, three solid regions are added. The first region is the 8 mm × 1.2 mm rectangular silicon based resistance heater which is the source of heat; the second region is the heater board upon which the heater is placed; the third part is the PWB substrate where the heater board is attached. The heater board is 48 mm long, 76 mm wide, 1 mm thick and the PWB substrate is 102 mm long, 76 mm wide, 5 mm thick. Hence, the physical model has two material states: fluid and solid. The entire physical model is meshed into triangular finite volume elements. The total number of element nodes is approximately 150,000. The model is not uniformly meshed. The center region close to the jet outlet is gridded much finer than the edge of the dome which facilitates the higher accuracy at the near jet exit region.

After the GAMBIT preprocess, the meshed model is imported into Fluent which is the CFD solver. At this step, the boundary conditions are defined. With the limitation of Fluent version 5.5, there is no moving wall boundary condition which can be applied at the vibration diaphragm. Kral's method, a velocity boundary condition, is used here instead [9]. As shown in Eq. (1), $f(\eta) = 1$ is set. The magnitude of the velocity U_0 is determined from the diaphragm displacement measurement by using a laser vibrometer. Based on the diaphragm deflection, the diaphragm dimensions and the vibration frequency, the volumetric flow rate in a half vibration cycle (i.e. the impingement cycle) can be calculated. Then the linear velocity magnitude U_0 at the diaphragm can be determined by the volumetric flow rate with respect to the diaphragm surface area. U_0 here for this ACS device is 0.1276 m/s. From Eq. (1), the velocity boundary condition varies not only with space, but also with time. Therefore, an unsteady simulation is applied. In one cycle, the averaged velocity at the vibrating diaphragm is zero to ensure zero net mass flux at that surface which meets the inherent nature of a synthetic jet. The second boundary condition is the outlet boundary condition which is set as the atmospheric pressure at the outside shell surface of the dome. The third boundary condition is added at the heat source. During the heat transfer measurement, the current through the heater and the voltage drop are monitored. Thus the power consumption on the heater (i.e. the heat generated by the heater) is known. In Fluent, this boundary condition is defined as the heat generation rate which is calculated by the power consumption density. All the interfaces between the solid (e.g. PWB) and fluid (e.g. air) are defined as the coupled walls. The substrate outside walls exposed to the stationary air are defined as the walls with natural convection.

Since different materials are involved in the simulations, the determination of the material physical properties is important. In the heat transfer modeling, for simplicity, the room temperature properties are used. In the temperature range of 20 °C and 100 °C, major air properties (i.e. density, specific heat, thermal conductivity and viscosity) vary less than 20%. Therefore, it is a reasonable assumption to apply air properties at room temperature to the simulations. There are three other solid materials. The heater is silicon based; thus, silicon material properties are used. The ACS PWB substrate is a FR4 (flame retardant) epoxy glass fiber composite material. From literature, its thermal conductivity is about 0.23 W/m K, specific heat is 1000 J/kg K, and density is 1500 kg/m^3 at room temperature. The physical properties of FR4 epoxy glass fiber may vary with temperature. However, the data at temperatures other than room temperature are not available, and hence temperature invariant properties are assumed. The heater board is different from the PWB substrate due to the presence of copper trace pattern on the board which can affect the value of the thermal conductivity. The thermal conductivity is corrected by Eq. (2) [11]:

$$k_{\mathrm{SUBS}} = \frac{0.25 t_{\mathrm{B}} + 13.65 C_{\mathrm{c}} t_{\mathrm{t}}}{t_{\mathrm{B}}} \tag{2}$$

where k_{SUBS} is the thermal conductivity of the substrate, t_{B} is the substrate thickness in mm, C_{c} is the fraction of conductor coverage, t_{t} is the trace thickness in oz (1 oz = 35.6 μm) of copper. On the heater board, the copper trace has the thickness of 22 μm and covers about 50% of the board area. The board thickness is about 1.6 mm. Thus, the thermal conductivity of the board is calculated to be about 3 W/m K.

After the boundaries are defined and the physical properties are applied, fluid mechanics model should be selected to solve the problems. Large eddy simulation is a promising approach for simulation of complex, high Reynolds number turbulent flows. In the LES approach, the turbulent scales are decomposed into large resolved scales (which are likely to be anisotropic) and subgrid unresolved scales (which may or may not be isotropic) by applying a spatial filter to the Navier–Stokes equations. The filtered Navier–Stokes equations represent the transport of the low

frequency modes in the resolved scale velocity field and include the contribution of the unresolved high frequency small scales through subgrid scale stress (SGS). The impact of the subgrid scales on the resolved scales is parameterized by the so-called subgrid scale model. Since only the large energy containing scales have to be resolved in LES, in principle, turbulent flows can be simulated at a higher Reynolds number and/or on a coarser grid resolution when compared to the direct numerical simulation approach. This is a main virtue of the LES approach.

There are two key characteristics in LES approach. One is the filter function; the other is the SGS model. First, the flow variables are decomposed into large-scale components (denoted by an overbar) and small subgrid scale components by employing a filtering operation. In Fluent, a finite volume method is applied to solve the differential equations. The finite volume discretization implicitly provides the filtering operation:

$$\bar{\phi}(x) = \frac{1}{V}\int_V \phi(x')\,\mathrm{d}x', \quad x' \in V \tag{3}$$

where V is the volume of a computational cell. The filter function, $G(x,x')$ implied here is then:

$$G(x,x') = \begin{cases} 1/V, & x' \in V \\ 0, & \text{otherwise} \end{cases} \tag{4}$$

Applying the filtering operation, the incompressible Navier–Stokes equations for the evolution of the large-scale motions are obtained. The resulting governing equations are

$$\frac{\partial \rho}{\partial t} + \frac{\partial \rho \bar{u}_i}{\partial x_i} = 0 \tag{5}$$

$$\frac{\partial}{\partial t}(\rho \bar{u}_i) + \frac{\partial}{\partial x_j}(\rho \bar{u}_i \bar{u}_j) = \frac{\partial}{\partial x_j}\left(\mu \frac{\partial \bar{u}_i}{\partial x_j}\right) - \frac{\partial \bar{p}}{\partial x_i} - \frac{\partial \tau_{ij}}{\partial x_j} \tag{6}$$

where i $(=1,2,3)$ indicates the spatial dimension; p is pressure; ρ and μ are the fluid density and viscosity, respectively; $\bar{u}_i(x_i,t)$ is the resolved velocity field; τ_{ij} is the subgrid scale stress defined by

$$\tau_{ij} = \rho\overline{u_i u_j} - \rho \bar{u}_i \bar{u}_j \tag{7}$$

The subgrid scale stresses resulting from the filtering operation are unknown and require modeling. The majority of the subgrid scale models in use today are eddy viscosity models. The models assume proportionality between the anisotropic part of the SGS stress tensor $\tau_{ij} - \frac{1}{3}\delta_{ij}\tau_{kk}$ and the resolved scale strain rate tensor $\overline{S}_{ij}$ as Eq. (8):

$$\tau_{ij} - \frac{1}{3}\delta_{ij}\tau_{kk} = -2\mu_t \overline{S}_{ij} \tag{8}$$

where μ_t is the subgrid scale turbulent viscosity, and $\overline{S}_{ij}$ is defined by

$$\overline{S}_{ij} = \frac{1}{2}\left(\frac{\partial \bar{u}_i}{\partial x_j} + \frac{\partial \bar{u}_j}{\partial x_i}\right) \tag{9}$$

The most basic of subgrid scale models is proposed by Smagorinsky and further developed by Smagorinsky [12] and Lilly [13]. In the Smagorinsky–Lilly model, the eddy viscosity μ_t is simulated by

$$\mu_t = \rho L_s^2 |\overline{S}| \tag{10}$$

$$\overline{S} = \sqrt{2\overline{S}_{ij}\overline{S}_{ij}} \tag{11}$$

where L_s is the mixing length of subgrid scales. Most of the other SGS models are the Smagorinsky type variations. In Fluent, the mixing length for subgrid scales L_s is computed using Eq. (12):

$$L_s = \min(\kappa d, C_s V^{1/3}) \tag{12}$$

where $\kappa = 0.42$, d is the distance to the closest wall, C_s is the Smagorinsky constant, and V is the volume of the computational cell. Lilly derives a value of 0.23 for C_s from the homogeneous isotropic turbulence in the inertial subrange. However, this value is found to cause excessive damping of large-scale fluctuations in the presence of mean shear or in transitional flows. $C_s = 0.1$ has been found to yield the best results for a wide range of flows and is the default value in Fluent. Based on the filter function and the Smagorinsky–Lilly SGS model, LES approach in Fluent can be applied to simulate complex fluid flows.

In order to combine the synthetic jet fluid mechanics simulation with heat transfer, a heat transfer model should be applied as well. Eq. (13) is the energy governing equation.

$$\frac{\partial}{\partial t}(\rho E) + \frac{\partial}{\partial x_i}(u_i(\rho E + p)) = \frac{\partial}{\partial x_i}\left(k_{\text{eff}}\frac{\partial T}{\partial x_i} - \sum_{j'} h_{j'} J_{j'} + u_i(\tau_{ij})_{\text{eff}}\right) + S_h \tag{13}$$

$$E = h_g - \frac{p}{\rho} + \frac{u_i^2}{2} \tag{14}$$

$$h_g = \sum_{j'} m_{j'} h_{j'} + \frac{p}{\rho} \tag{15}$$

$$h_{j'} = \int_{T_{\text{ref}}}^{T} C_{p,j'}\,\mathrm{d}T \tag{16}$$

where k_{eff} is the effective thermal conductivity, $J_{j'}$ is the diffusion flux of the species j', τ_{ij} is the subgrid scale stress defined by Eq. (8). The first three terms on the right hand of Eq. (13) represent energy transfer due to conduction, species diffusion, and viscous dissipation, respectively. S_h includes heat of chemical reaction and any other volumetric heat sources. Since the heat carrying fluid is air and its physical properties are close to the room temperature conditions in most of the modeling regions, the reference temperature is selected at 298.15 K.

In summary, there are three governing equations to solve this simulation problem. Eq. (5) is the law of conservation of mass. Eq. (6) is the Navier–Stokes equations which represent the momentum conservation. Eq. (13) is the law of energy conservation. LES approach is applied to simulate the fluid mechanics. The heat transfer model covers both conduction and convection. This is a complex

CFD modeling problem. In this research, a convergence acceleration approach, addition of complexity, is applied. This improves the solver performance by sequentially imposing the required complexities in the problem. For the fluid mechanics and heat transfer problems, the heat conduction is a time limiting step if the two calculations are performed simultaneously. As a result, heat transfer can be carried out first without fluid mechanics. After certain time (i.e. 625 s was used in these simulations), fluid mechanics is added to the calculation and both of them are conducted simultaneously. This approach can dramatically reduce the heater temperature ramping up time, and speed up the convergence process without losing the accuracy. Note that this addition of complexity approach exactly matches the heat transfer experimental sequences. First, the heater is heated up without the jet; second, the jet is turned on and the system reaches a steady state. By applying the addition of complexity approach, the simulations can be completed much more rapidly.

3. Simulation results and discussion

The grid and time step independence tests are performed on the 3-D model. Three different grids-90,000, 150,000, 200,000 and three different time steps-12, 16, 24 have been tested. 150,000 meshed nodes and 16 time steps per cycle can show satisfactory results which ensure the grid and time step independent. Due to the use of the addition of complexity approach, the first time step has a long time interval (i.e. 625 s). Then starting from the second time step, the time interval is reduced down to 0.000625 s to capture the detailed periodic fluid physics of the synthetic jets. To increase the accuracy, a 3-D double precision solver is applied to perform the fluid mechanics and heat transfer combined simulations.

During the course of the simulations, two variables are monitored. One is the local average heat transfer coefficient on the top surface of the heater array. The other one is the centerline velocity magnitude at 0.8 mm away from the jet exit. The results are shown in Figs. 4 and 5, respectively.

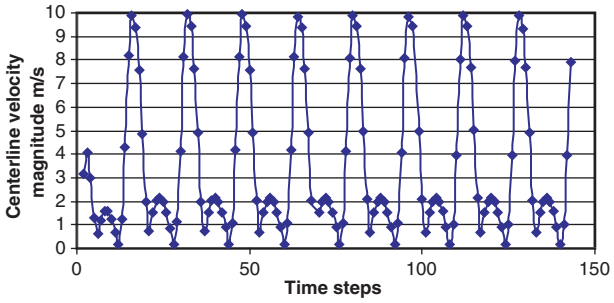

Fig. 5. The centerline velocity magnitude at the location of 0.8 mm away from the jet exit during the simulation process for ACS with the fluidic channel exit having dimensions of 5.08 mm × 1.00 mm.

From both figures, it is observed that the simulation results become convergent almost after the first cycle. The simulation results are compared with the actual experimental data obtained from previous research [6]. The simulated local heat transfer coefficient has a small fluctuation within one cycle. The average is about 97 W/m^2 K. The experimental value from infrared thermography mapping is about 80 W/m^2 K. The discrepancy is about 21%, which may be a result of the assumed temperature independence of the materials properties. The room temperature assumption "exaggerates" the cooling capacity of the air jets (i.e. in reality the air is heated as it passes above the heater), resulting in the simulated heat transfer coefficient is higher than the experimental result. In addition, the incompressible gas assumption may not be accurate for the gases existing in the cavity.

Fig. 5 illustrates that the centerline velocity magnitude is cycling periodically. The simulation results are also compared with the same spot hot-wire measurement data as shown in Fig. 6. There are a good match at the impingement stroke, and some discrepancies at the intake stroke. The heat transfer simulations can be compared with the experimental data by the temperature distribution. Fig. 7 shows good agreement between the simulations and the experiments on the temperature distribution along the centerline of the board top surface. The origin point on the

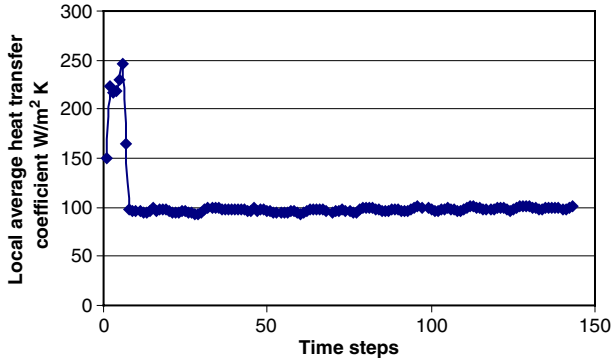

Fig. 4. The local average heat transfer coefficient on the heater during the simulation for ACS with the fluidic channel orifice, 5.08 mm by 1.00 mm in dimensions.

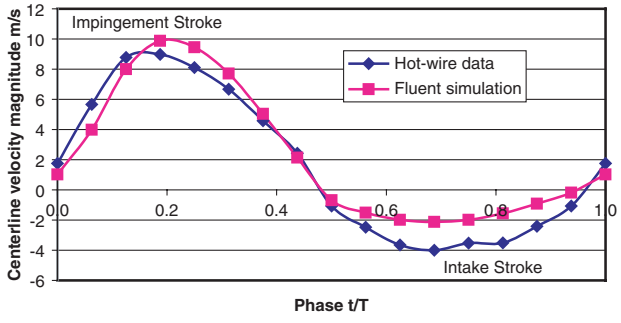

Fig. 6. Comparison between Fluent simulation and hot-wire measurement for ACS with the fluidic channel exit having dimensions of 5.08 mm × 1.00 mm.

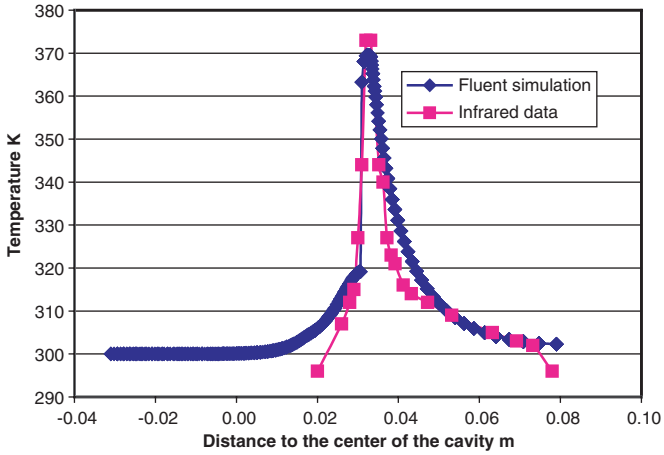

Fig. 7. Comparison of temperature distribution on the device top surface for ACS with the fluidic channel exit having dimensions of 5.08 mm × 1.00 mm.

x-axis of Fig. 7 is defined as the orifice exit. These velocity and temperature comparisons verify that the fluid mechanics and heat transfer simulations have the ability to reflect the experimental data.

One major application of CFD simulations is to use the developed model in the engineering predictions. The methodology developed for 5.08 mm × 1.00 mm fluidic channel is applied to project the behavior of another ACS structure, a fluidic channel with a rectangular exit of 10.00 mm × 1.00 mm in this section.

The second ACS model is similar to the first one, in that the same solid substrate volume and the same dome volume are used for the jet development. The only difference is that the fluidic channel cavity embedded inside the device is enlarged. Therefore, some solid volume turns into void fluidic channel volume. Due to the similar mesh density in that region, the entire second ACS is meshed into the similar nodes, 150,000. The model cross-section view looks the same as Fig. 3. The velocity boundary condition, the material properties, LES turbulence model, and the addition of complexity solving approach are the same as the previous section. Figs. 8–11 present the simulation results.

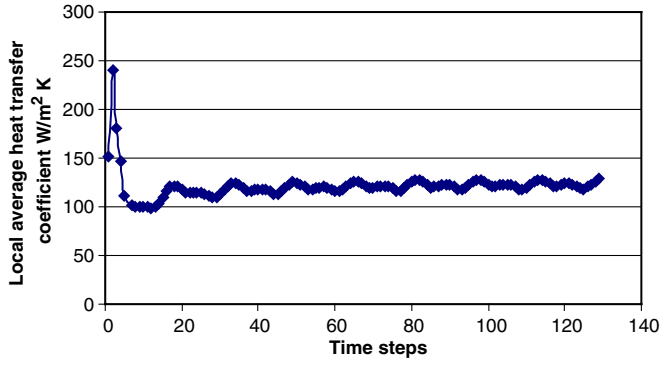

Fig. 8. The local average heat transfer coefficient on the heater during the simulation for ACS with the fluidic channel exit having dimensions of 10.00 mm × 1.00 mm.

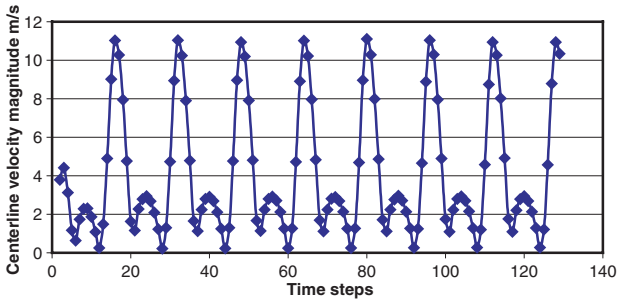

Fig. 9. The centerline velocity magnitude at the location of 0.8 mm away from the exit during the simulation process for ACS with the fluidic channel exit having dimensions of 10.00 mm × 1.00 mm.

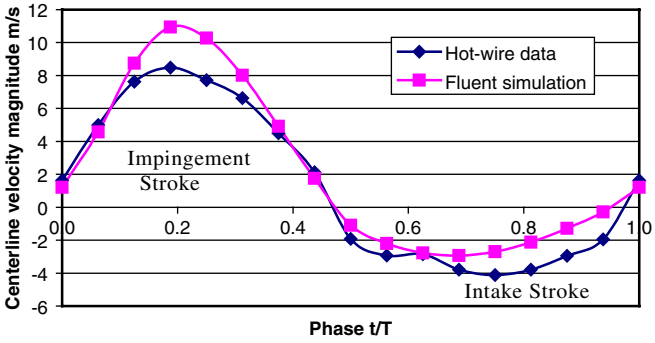

Fig. 10. Comparison between Fluent simulation and hot-wire measurement at 0.8 mm away from exit for ACS with the fluidic channel exit having dimensions of 10.00 mm × 1.00 mm.

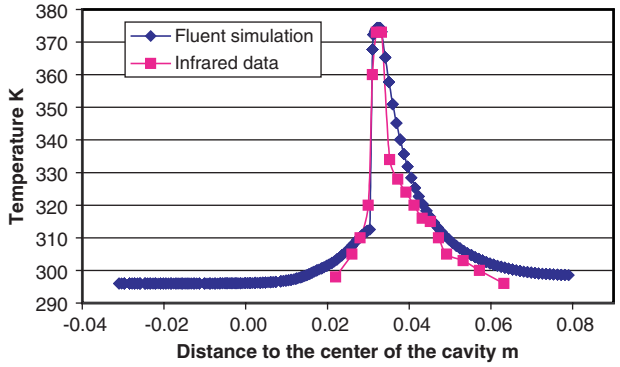

Fig. 11. Comparison of temperature distribution on the device top surface for ACS with the fluidic channel exit having dimensions of 10.00 mm × 1.00 mm.

Figs. 8 and 9 demonstrate that after the first cycle, the simulation is stabilizing to a convergent result. Fig. 10 shows the centerline velocity magnitude comparison at 0.8 mm away from the exit. Fig. 11 is the temperature distribution comparison on the top surface of the ACS substrate. All the comparisons show consistent results with the experiments. The final local average heat transfer coefficient on the heater determined from model prediction is approximated 123 W/m^2 K. This is in good agreement with the experimental heat transfer coefficient of 127 W/m^2 K. Therefore, it has been demonstrated that the CFD

approach can be employed to predict the synthetic jet behavior.

4. Conclusions

In this study, CFD software, Fluent, is employed to solve the complicated synthetic jet fluid mechanics coupled with heat transfer problem. To accomplish the numerical simulations, some necessary simplification assumptions are applied. The vibration diaphragm boundary condition is simulated as a sine wave velocity boundary. The physical properties of air and PWB are assumed to be temperature independent. The LES turbulence model is used instead of a direct numerical simulation. Addition of complexity allows the simulations to be accomplished in a reasonable computation time. CFD models exhibit satisfactory accuracy compared with experimental results on synthetic jet velocities, PWB temperature distributions and jet heat transfer coefficients. Therefore, this research provides a valid and practical CFD numerical approach to solve the synthetic jet fluid mechanics and heat transfer problem.

References

[1] B. Smith, A. Glezer, The formation and evolution of synthetic jets, Phys. Fluids 10 (9) (1998) 2281–2297.
[2] R. Rathnasingham, K. Breuer, Coupled fluid-structure characteristics of actuators for flow control, AIAA J. 35 (5) (1997) 832–837.
[3] O. Rediniotis, J. Ko, X. Yue, A. Kurdila, Synthetic jets, their reduced order modeling and applications to flow control, in: Proceedings of 37th Aerospace Sciences Meeting and Exhibit, Reno, NV, 1999, AIAA99-1000.
[4] Y. Wang, S. Bidstrup, G. Yuan, M. Allen, Printed-wiring-board microfluidics for thermal management of electronic systems, in: Proceedings of 2002 ECS International Symposium, Philadelphia, PA, 2002, pp. 161–170.
[5] Y. Wang, G. Yuan, Y. Yoon, M. Allen, S. Bidstrup, A MEMS active cooling substrate for microelectronics thermal management, in: Proceedings of 2003 ASME International Mechanical Engineering Congress and R&D Exposition, Washington, DC, 2003, IMECE2003-42799.
[6] Y. Wang, G. Yuan, Y. Yoon, M. Allen, S. Bidstrup, Active cooling substrates for thermal management of microelectronics, IEEE Trans. Compon. Pack. Technol. 28 (3) (2005) 477–483.
[7] D.P. Rizzetta, M.R. Visbal, M.J. Stanek, Numerical investigation of synthetic-jet flowfields, AIAA J. 37 (8) (1999) 919–927.
[8] C.Y. Lee, D.B. Goldstein, Two-dimensional synthetic jet simulation, in: Proceedings of 38th Aerospace Sciences Meeting and Exhibit, Reno, NV, 2000, AIAA 2000-0406.
[9] L.D. Kral, J.F. Donovan, A.B. Cain, A.W. Cary, Numerical simulation of synthetic jet actuators, in: Proceedings of 28th AIAA Fluid Dynamics Conference/4th AIAA Shear Flow Control Conference, Snowmass Village, CO, 1997, pp. 97–1824.
[10] V.A. Chiric, T.T. Lee, J.L. Rosales, A novel cooling enhancement in microelectronic devices and systems using oscillatory impinging air jets, in: Proceedings of 2001 ASME International Mechanical Engineering Congress and Exposition, New York, NY, 2001, IMECE2001/HTD-24391.
[11] J.E. Sergent, S. Al Krum, Thermal Management Handbook for Electronic Assemblies, McGraw-Hill, New York, 1998, p. 3.16.
[12] J. Smagorinsky, General circulation experiments with the primitive equations. I. The basic experiment, Mon. Weather Rev. 91 (1963) 99–164.
[13] D.K. Lilly, On the application of the eddy viscosity concept in the inertial subrange of turbulence, NCAR Manuscript, 1966, p. 123.